

RADIOLYTIC CORROSION OF CU NUCLEAR WASTE CONTAINERS

Balsam Ibrahim¹, Dmitrij Zagidulin¹, Jared M. Smith², Sridhar Ramamurthy³, J. Clara Wren¹, David W. Shoemsmith^{1,3}

¹Department of Chemistry, Western University, 1151 Richmond St., LON, ON, N6A 3K7, Canada

²Canadian Nuclear Laboratories, Chalk River, Ontario, Canada

³Surface Science Western, Western University, 999 Collip Circle, LON, ON, N6G 0J3, Canada

ABSTRACT

The corrosion of copper is being studied under the aerated vapour conditions which could prevail in the early period after nuclear waste container emplacement in a deep geologic repository. Exposure experiments are being conducted at two relative humidities (70% and 85%) in the presence and absence of a low γ -radiation dose rate (0.35 Gy/h). Corrosion is observed to occur generally across the surface yielding a film of Cu_2O , the surface of which eventually becomes oxidized to CuO . This process is accelerated by the presence of a radiation field. The breakdown of this layer leads to dissolution as Cu^{2+} and its redeposition to form CuO . This conversion process spreads across the surface rather than penetrating into it and appears also to be accelerated by the presence of radiation. At the higher relative humidity some pitting occurs. The absence of cupric nitrate deposits shows that, despite the formation of nitric acid, no nitrogen fixation occurs.

Keywords: vapour phase corrosion of copper, low γ -radiation fields, influence of relative humidity, spent fuel disposal.

1. INTRODUCTION

The long-term management plan for spent nuclear fuel in Canada is to bury it at a depth of ~ 500 m in a deep geologic repository (DGR) [1]. This repository will be designed according to a multiple barrier concept in which the fuel bundles will be sealed in a corrosion-resistant container (UFC) and then emplaced in boreholes subsequently backfilled with bentonite clay, as illustrated schematically in Figure 1. The chosen UFC involves a dual-walled container fabricated with an inner carbon steel load-bearing vessel with an outer Cu corrosion barrier [2]. Originally, the Cu corrosion barrier was designed with a thickness of 25 mm. However, available corrosion models estimate that only ~1.27 mm of Cu is required to avoid failure by corrosion in the anticipated environment [2,3]. For such a container the influence of water radiolysis (due to the decay of radionuclides in the fuel) was calculated to be negligible.

More recently, a thinner walled container has been adopted in an effort to avoid design issues associated with its fabrication and welding. Such a design revives the possibility that γ -radiation could influence the corrosion of the Cu barrier by producing radiolytic oxidants in the aqueous environment surrounding the container. This makes a more thorough assessment of the potential corrosion damage a key requirement for licensing. The dose rate anticipated on the surface of a thin walled container could initially be in the range of ~ 5 Gy/h and would decay to ~ 0.44 Gy/h over a period of 200 years based on the half life of the dominant γ -emitter in the fuel (^{137}Cs) [4]. The primary goal of this project is to determine the influence of γ -radiation on Cu corrosion under DGR conditions, which will allow a more accurate assessment of the possible extent of corrosion damage sustainable over its emplacement lifetime. This is an essential requirement if an adequate Cu corrosion barrier thickness is to be specified.

After emplacement, containers will experience a sequence of exposure environments in a DGR: 1) an initial aerated period with no condensed H_2O on the Cu surface; 2) a period of aerated vapour in equilibrium with condensed H_2O on the surface; 3) a transition period to fully saturated, potentially oxidizing aqueous conditions; and 4) a final aqueous anoxic period after the available O_2 has been

consumed by container corrosion, and by reactions with minerals and organic matter in the clay. While the rate of corrosion in period 1 is expected to be minimal, the corrosion rates could be significant throughout periods 2 to 4. This paper will focus on the influence of radiation on Cu corrosion in period 2 when the effect of radiation is expected to be most significant.

In period 2, it is anticipated that the temperature at the canister surface will be in the range of 70 to 100 °C due to radioactive decay processes within the fuel [5]. During this period a relative humidity (RH) of ~75 % is likely to be present in the clay at the surface of the container and subjected to a γ -radiation field on the outside of the container. The γ -radiolysis of liquid water leads to the formation of highly reducing and oxidizing species such as $^{\bullet}\text{OH}$, e_{aq}^{-} , H^{\bullet} , H_2 , H_2O_2 , and H^+ with the most stable and highly oxidizing species being H_2O_2 . However, predicting the radiolysis products in thin H_2O layers in contact with humid air is more challenging since over 700 reactions and 75 species are involved. Most importantly, since N_2 is present, oxidants such as HNO_3 , NO_2 and N_2O will be formed [4].

Vapour phase corrosion studies (period 2) are being undertaken in a controlled environment to simulate the temperature and humidity anticipated during this period. Experiments are being performed in both the presence and absence of a radiation field, the purpose of the latter being to establish a baseline against which to gauge the influence of radiation. While there is extensive literature on atmospheric corrosion, little is known about the corrosion of Cu in the anticipated repository conditions.

Atmospheric studies have shown that Cu_2O forms rapidly on Cu surfaces with the oxide achieving a thickness of 100 to 150 nm [6]. Similarly, extensive studies on the formation of corrosion patinas have shown that a cuprite layer (Cu_2O) initially forms on the copper surface followed by its partial conversion to Cu^{2+} [7] the latter being a process thought to require the presence of water. DeNardis et al. studied film growth on Cu in aqueous solutions containing H_2O_2 , which can perhaps be taken to represent irradiated condensed layers of water. The early stages of Cu oxidation involve the chemisorption of an oxide precursor, such as O_2 , followed by nucleation and growth of oxide islands [8]. Cuprite (Cu_2O) is formed first on the surface since it is thermodynamically favoured. Once the surface is covered by Cu_2O , further oxidation can occur yielding Cu^{II} oxides and a duplex film is produced with $\text{CuO}/\text{Cu}(\text{OH})_2$ on top of the Cu_2O layer [9].

Studies on the direct effects of γ -radiation on the corrosion of Cu are sparse [10,11]. Corrosion was observed in irradiated moist air with the extent of corrosion damage increasing with the moisture content of the gas phase [10]. In experiments at high dose rates (0.7 to 2 kGy/h), temperatures in the range 90 °C to 150 °C, and relative humidities (RH) ranging from 0% to 100%, the appearance of the corroded surface changed with RH from a light tarnish in dry air, to brown/yellow at 15% RH and then to a black/brown scale at 100% RH. Using X-ray diffraction, it was shown that, after exposure at 150 °C small amounts of Cu_2O and $\text{Cu}_2\text{NO}_3(\text{OH})_3$ were present at 0 %RH, Cu_2O and some $\text{Cu}_2\text{NO}_3(\text{OH})_3$ at 15% RH, and Cu_2O , with some CuO , but no $\text{Cu}_2\text{NO}_3(\text{OH})_3$ at 100% RH. Minor pitting was also observed at 100% RH.

It was concluded that the formation of $\text{Cu}_2\text{NO}_3(\text{OH})_3$ could be attributed to the presence of nitrogen oxides and nitric acid generated by radiolysis and its formation as a non-protective deposit was associated with pitting. The greater corrosion rates observed in moist environments compared to dry air were attributed to the formation of radiolytic oxidants in the gas phase which then concentrate in the thin film of water on the corroding surface [11]. Comparison of the effects of radiation on Cu corrosion at a dose rate of 10 kGy/h in aqueous and moist air environments showed more severe corrosion occurred in the vapour phase [12].

2. EXPERIMENTAL

Coupons were cut from P-deoxidized wrought Cu supplied by the Swedish Nuclear Fuel and Waste Management Company (SKB, Stockholm, Sweden). The coupons were polished successively with 600 and 1200 grit SiC paper on all 6 sides, washed and ultrasonically cleaned in Type I water and methanol

for 2 minutes, and then washed again with Type I water before being dried using ultrapure Ar gas. The polished coupons were placed in a desiccator for one day to dry, and then their dimensions and weight recorded prior to exposure.

Two sets of experiments are underway. In one set the coupons were placed on a Teflon holder with a 1 cm² face facing upwards and the holder placed in a humidity chamber (Associated Environmental Systems) set to 75 °C and 70% RH. A schedule was set to remove coupons after 1d, 2d, 7d, 14d, then approximately monthly up to 1 year of exposure. On removal from the chamber the coupons were dried with Ar gas, and placed in a desiccator for one day. Subsequently, they were weighed and stored in a glove box to avoid air oxidation, before eventual analysis using Raman spectroscopy and SEM. A second set of experiments was performed in an oven at 75 °C at Canadian Nuclear Laboratories, Chalk River, Ontario in both the presence and absence of a radiation field. In these experiments the coupons were placed on a Teflon holder with a 1 cm² face facing upwards. This holder is placed in a 1L glass bottle. A second glass bottle, containing distilled water is used to create the required humidity by cooling the water to 70 °C. Humidified air is made to flow from this vessel at a flow rate of 5 ml/min to achieve 85% RH in the test vessel. A dose rate of 0.35 Gy/h is provided by a ⁶⁰Co γ -source, with one set of coupons shielded from this field behind lead blocks. Coupons were removed after 50.8 d and 103.7 d of exposure (corresponding in the irradiated cases to total radiation doses of 424.6 Gy and 866.2 Gy, respectively).

A Renishaw 2000 Raman spectrometer equipped with a 633 nm He-Ne laser was used with a 50x objective to focus on features of the corroded surfaces. Spectra were taken in the range 120-2000 cm⁻¹ (some to 4000 cm⁻¹), at 0.5 mW of power. Spectra were calibrated using the 520.5 cm⁻¹ line of a silicon wafer.

Micrographs of the Cu coupons were recorded on a Hitachi S4500 SEM equipped with an EDX analyzer used to elucidate the elemental composition of the surfaces. SEM images were taken using an accelerating voltage of 5.0 kV and at magnifications from 100 to 20,000x. SEM images and EDX spectra were taken of representative areas and any unique features on the coupons. A Zeiss 1540 XB instrument equipped with a 30 kV Ga ion beam was used to cut focused-ion beam (FIB) cross-sections and imaging was performed at an angle of 54°.

3. RESULTS AND DISCUSSION

3.1 Experiments in the presence of a low γ -radiation dose rate (RH 85%)

The data from the low dose γ -radiation study exhibit two distinct corrosion features; (i) the general corrosion of the majority of the surface (termed the general area); and, (ii) a number of apparently more heavily corroded areas (termed patches). These areas are clearly distinguishable in the optical images in Figure 2, the generally corroded area appearing as copper-coloured and the patches as purple/blue locations. The influence of γ -radiation on general corrosion is clear in a comparison of the SEM micrographs of the irradiated and non-irradiated surfaces, Figure 2. After 51 days exposure the irradiated surface appears more extensively corroded and after 104 days both surfaces are covered with a layer of nodular deposits. These nodules are denser and larger on the irradiated than on the unirradiated surface, indicating an accelerated corrosion process. Comparison of the surfaces from the short (51 d) and long (104 d) experiments show the corrosion process has progressed in both cases but particularly so for the irradiated coupon.

Although not shown, examination of FIB-cut cross sections shows the surface film on the general area to be ~200 nm thick after 104 d of exposure for both the irradiated and non-irradiated samples. This is consistent with published studies that report similar film thicknesses after several days of exposure in a non-irradiated atmosphere [6]. This layer appears to be protective and, if so, its faster growth in the presence of γ -radiation would be beneficial.

Inspection of the optical images shows the darker patches cover a larger area of the surface after the longer exposure with their growth progressing predominantly along the polishing lines in the surface. The influence of γ -radiation on the size of the patches is clear after 104 days, the irradiated surface possessing a greater number of patches after both exposure periods, Figure 3. Their areal dimensions are also greater indicating their growth has been accelerated by the presence of irradiation.

The SEM micrographs, Figure 3, show that, compared to the general surface, the corrosion product within the patches is denser and more copious, indicating more extensive corrosion at these locations. Additionally, the corrosion product forms larger nodules in the presence of γ -radiation. Whether or not this is a consequence of deeper penetration at this location or just a difference in porosity of the deposit remains to be determined.

A possible explanation for the formation of these more heavily corroded patches is that they are a consequence of condensed water on the surface. It has been reported that for a critical RH, typically in the range 50 to 70%, the condensation of H₂O is to be expected [13]. At the 85% RH employed in this study, condensation of water almost certainly occurred. The optical images and differences in corrosion product morphology between the general areas and the patches suggest the surface did not wet uniformly, the patches indicating the more extensive corrosion process as a consequence of the formation of water droplets at that location.

In a thin condensed aqueous film corrosion occurs electrochemically and can proceed more rapidly than in a gaseous environment. Also, corrosion in thin films can be more severe than in the bulk solution since the transport path for O₂ dissolved in the film is short making its flux from the water/atmosphere interface to the corroding surface more rapid than in bulk solution and preventing the transport limitation of the cathodic reaction (O₂ reduction) commonly encountered in aqueous environments [14]. In the presence of γ -radiation more aggressive oxidants, such as H₂O₂ and HNO₃ will form and subsequently concentrate in condensed water layers. The establishment of these more aggressive oxidizing conditions would account for the enhancement of corrosion observed in the patches.

Patches, irrespective of whether γ -radiation was present or not, grew with a central accumulation of corrosion product. In optical images this can be seen as a central dark spot within the patch, and in SEM micrographs as an accumulation of larger globular deposits as shown in Figure 4. As shown in the figure, this accumulation tends to be concentrated along the original polishing lines. This choice of location could be dictated by two features: the more likely accumulation of water within the polishing grooves, and/or the greater likelihood of stress-induced fracture of the more general corrosion film initially forming at this location.

The suspicion that the extent of corrosion at these locations is greater is confirmed by the SEM micrographs recorded on FIB-cut cross sections. Figure 5 shows the thickness of the corrosion product varies with location from 234 nm at the thinnest location to 2.62 μ m at the thickest location. Additional cross sections (not shown) cut \sim 50 μ m inside and outside the patch showed that the film thickness varied from \sim 60 nm to 176 nm at locations in the general area to 160 nm to 390 nm within the patch. Inspection of the metal/deposit interface shows that, despite these differences in thickness of the deposit, the observed depth of corrosion penetration into the metal is only slightly greater beneath the thicker than the thinner deposit.

In the absence of a significant bulk solution the transport of soluble Cu cations (most likely as Cu²⁺ which is more soluble than Cu⁺) will be limited, and corrosion product deposition would occur at the corrosion site. Consequently, this difference in penetration depth and film thickness at the same location can be taken as an indication of the extensive porosity in the deposit, a small volume of metal having been converted to a large volume of corrosion product oxide/hydroxide. The aspect ratios (the ratio of the depth of corrosion to the area corroded) are extremely small indicating that corrosion spreads laterally rather than penetrates deeply.

A similar FIB cross section cut through the central mass of corrosion product within a patch on the unirradiated sample (after 104 d of exposure), Figure 6, shows both a thicker deposit (up to 3.33 μm) and an apparently greater depth of corrosion penetration than on the irradiated sample exposed for the same duration. A number of additional features are also visible; (i) the deepest penetration is not beneath the thickest deposit; (ii) considerable void space exists both in the deposit and along the deposit metal interface. Beyond this more heavily corroded region (towards the left edge of the FIB section) the penetration depth is limited to ~ 633 nm which is similar to the penetration depths observed on the irradiated sample at locations away from the central core of the patch.

These two analyses suggest deeper corrosion penetration occurs in the absence of irradiation. However, this would be a premature conclusion on the basis of only two cross-sectional analyses. A more likely explanation is that while the general distribution of corrosion is greater in the presence of irradiation the depth of penetration at the centre of the patch is predominantly dependent on the presence of condensed water at that location.

EDX analyses of the cross-sections, Tables 1 and 2, show the Cu to O ratio varies with depth in the oxide deposit. While it is likely that these analyses contain an interference from the substrate metal, they show a lower ratio at the outer surface than closer to the corrosion product/metal interface. The high Cu/O ratios indicate the film is probably Cu_2O with the low ratio at the outer surface of the unirradiated sample (1.6) suggesting the presence of CuO . These claims are supported by Raman spectra (not shown) of both the general area and patches in both conditions, which have peaks at 147, 220, 525 and 625 cm^{-1} that are readily assigned to Cu_2O [15,16] and a peak at 290 cm^{-1} that confirms the presence of CuO [17]. Note that no N-species were detected by Raman spectroscopy on the irradiated samples despite the likely formation of HNO_3 . This observation is consistent with the literature reporting the absence of $\text{Cu}_2\text{NO}_3(\text{OH})_3$ at higher RH [10].

XPS analysis, Table 3, which analyzes only the outer surface of the films and, for the film thicknesses shown, would not detect the Cu substrate, shows Cu(II) is the dominant Cu oxidation state on the surface of both the general areas and the patches. Coupled with the Raman analyses this would suggest the corrosion product in both areas is comprised of an inner Cu_2O layer with the outer surface being CuO . XPS also showed that O was present predominantly as OH ($\sim 75\%$) suggesting the possible presence of $\text{Cu}(\text{OH})_2$ although this would need to be confirmed.

3.2 Corrosion experiments in unirradiated humid atmospheres (RH 75%)

A similar analysis was performed on specimens exposed in the humidity chamber with both general corrosion and more extensively corroded patches being analyzed. Presently a full analysis of exposed samples has not been completed. Figure 7 shows a series of optical images and SEM micrographs recorded after 7, 150 and 360 days of exposure (70 $^\circ\text{C}$, 75% RH). After 7 days only a few small dispersed globular features are observed with a noticeable increase after 14 days. After 150 days the deposit is more uniform, although the optical image of the surface after 360 days shows the presence of such deposits can be patchy.

Inspection of the coloured patches shows their number and size appears to be random up to 180 days beyond which their number steadily increases. After 240 days the surface is covered with small patches, but after 360 days there is an increased number of enlarged patches which may be a series of coalesced smaller ones, as shown in the optical images. As observed in the irradiated experiments, the extent of corrosion was greater within the patches than in the general areas, with an increased density and size of deposited product. As observed in the irradiated study the patches of enhanced corrosion appeared to progress along the polishing lines.

Figure 8 shows a more extensive analysis of both a general area and a patch after 30 days of exposure. The more extensively corroded patch analyzed is indicated by the circle in the optical image, Figure 8(a). In the general area, Figure 8(b) the surface is uniformly oxide covered with small areas of clustered ill-

defined crystals. It is likely that these small clusters are the sites at which breakdown of the surface film occurred followed by the subsequent deposition of a corrosion product leading to repair of the site. Within the patch, Figure 8(c) the corrosion deposit is more copious and in the form of accumulated crystals indicating some local aqueous transport prior to deposition. This suggests the presence of condensed water at these locations despite the lower RH (70%) in these experiments compared to the irradiated experiments (85% RH).

FIB cross sections were cut at the centre of the patch (the lighter area in the optical image) and across the border between a patch and a generally corroded area (as indicated by the line in the optical image, Figure 9(a). Near the centre the thickness of the corrosion product was in the range 300 to 475 nm (not shown). Across the border between the patch and the generally corroded area (the darker area), the film was 389 nm thick within the patch, Figure 9(c). Outside the patch the film may be considerably thinner as indicated by the 120 nm scale marker. Presently, the location of the Cu/film boundary is uncertain, but may be located just below the voids visible at approximately the same depth at both locations. If this proves to be the boundary then the film thickness inside and outside the patch may be the same, and the 120 nm scale marker in Figure 9(b) may indicate the location of an outer oxide with different properties/composition to the thicker sublayer. Additional cross sections are under investigation to identify unequivocally the location of the interface. Irrespective of this uncertainty, the penetration depths within the patches appear to vary little across the patch, again demonstrating that corrosion spread across the surface rather than penetrated into it. Additionally the depth of penetration in the general areas and within the patches are similar to those observed on the irradiated samples (discussed above), except for the absence of the more deeply penetrated central spots covered by a much thicker deposit.

Raman spectra recorded on the sample exposed for a 30 day period, Figure 8(d) show the peaks at 147, 220, 525 and 625 cm^{-1} demonstrating the presence of Cu_2O in both the generally corroded areas and the patches. However, after 30 days CuO , indicated by a peak at 297 cm^{-1} , is only observed within the patches, Figure 9(d). Raman spectra recorded on samples exposed for 60 and 90 days show that a weak CuO Raman signal is observed on the surface of the general area, only a few locations being free of CuO . In addition the CuO Raman signal for locations within the patches becomes stronger. These observations indicate that the general oxidation of the surface increases with time of exposure. These differences persist over the longer exposure periods. As observed for the irradiation experiments, XPS shows Cu(II) to be the dominant Cu oxidation state in both areas (87%), Table 3. This is higher than the 75% for Cu(II) observed in the higher RH experiments with and without irradiation, and suggests that the conversion of the outer regions of a Cu_2O film to CuO is more readily achieved at the lower RH.

3.3 The influence of relative humidity and irradiation

The two clear influences on the corrosion process are relative humidity and irradiation, of which that of relative humidity appears to be the most important. The general features of the corrosion process are the same at both RH employed and irrespective of whether radiation is present or not. The surface undergoes a general corrosion process leading to the formation of a layer of Cu_2O which is subsequently partially further oxidized to CuO at the outer oxide/vapour phase interface. This process appears to be limited in the humidity chamber experiments at the lower RH of 70%. This suggests these locations may be passive with the conversion of Cu_2O to CuO limited in the absence of condensed water. At the higher RH, the presence of γ -radiation accelerates the formation of this layer.

Condensation of water at some locations leads to the dissolution and transport of Cu^{2+} , which is more soluble than Cu^+ . Since the amount of condensed water is limited, particularly in the humidity chamber experiment, dissolved Cu^{2+} is immediately redeposited. With time the area of the surface covered with redeposited CuO increases as the patches spread leading to an increased area of the surface covered by $\text{Cu}_2\text{O}/\text{CuO}$. The aspect ratio of these patches (depth of penetration/area corroded) is very small demonstrating that the dominant mode of damage accumulation is the spreading of corrosion rather than its penetration into the metal.

For this to be the case the dominant location of corrosion must be at the periphery of the spreading patches. Since the general surface corrosion process is dominated by the formation of Cu₂O while that within the patches involves dissolution of Cu²⁺ and its redeposition as CuO, the most likely process driving the spread of patches is the oxidation of Cu₂O to Cu²⁺ in locally condensed water. Since the transport range of dissolved Cu²⁺ is limited its redeposition occurs close to the site at which it is formed. In the low humidity experiment this leads to the accumulation of a compact layer of small crystals. At the higher humidity the accumulation of deposit is thicker and the crystals more poorly formed.

At the higher RH the spread of patches of redeposited CuO occurs around a small central region which undergoes pit formation leading to deeper penetrations into the Cu. This suggests a breakdown of the Cu₂O layer at this location. This pitting is only observed at the lower RH after prolonged exposure (150 d) but occurs at the higher RH irrespective of whether a radiation field is present. These observations indicate that the main factor driving pit formation is the presence of accumulated condensed water, which occurs more readily at the higher humidity. However, the spread of such areas covered by deposited corrosion product (patches) appears to be accelerated by the presence of radiation. Although a more extensive analysis remains to be performed, there is presently no evidence that the low radiation dose rate employed in this study leads to a deeper penetration of corrosion into the Cu metal.

4. ACKNOWLEDGEMENTS

This research is funded by a Collaborative Research and Development grant supported by NSERC and the Nuclear Waste Management Organization (NWMO). We would like to acknowledge Dr. James Noel for helping design and set-up the radiation study conducted at the Chalk River Nuclear Laboratories, Dr. Jian Chen for assistance with the humidity chamber experiment, Dr. Mark Biesinger for XPS analysis, Mary Jane Walzak and Brad Kobe for assistance with Raman spectroscopy and SEM, analyses, respectively, and Dr. Todd Simpson for help with the cutting of FIB cross-sections. Balsam Ibrahim is grateful to Canadian Nuclear Laboratories (Chalk River) for student travel assistance.

REFERENCES

1. NWMO. "Learning More Together: Triennial Report 2011-2013"; Toronto, Ontario, 2013.
2. Kwong, G. M.. "Status of corrosion studies for copper used fuel containers under low salinity conditions"; NWMO TR-2011-14; Toronto Ontario, 2011.
3. King, F.. "Overview of the corrosion behaviour of copper and steel used fuel containers in a deep geologic repository in the sedimentary rock of the Michigan Basin, Ontario"; 06819-REP- 01300-10101 R00; 2005.
4. King, F.; Ahonen, L.; Taxen, C.; Vuorinen, U.; Werme, L.. "Copper corrosion under expected conditions in a deep geologic repository"; SKB TR-01-23; 2001.
5. Taxén, C.. "Atmospheric Corrosion of Copper 450 Metres Underground. Results from Three Years Exposure in the Äspö HRL", Mat. Res. Soc. Symp., 2004.
6. Odnevall, I.; Leygraf, C.. "Atmospheric corrosion of copper in a rural atmosphere". *J. Electrochem. Soc.* **1995**, *142* (11), 3682-3689.
7. FitzGerald, K. P.; Nairn, K.; Skennerton, G.; Atrens, A.. "Atmospheric corrosion of copper and the colour, structure and composition of natural patinas on copper". *Corros. Sci.* **2005**, *48*, 2480-2509.
8. DeNardis, D.; Rosales-Yeomans, D.; Borucki, L.; Philipossian, A.. "Characterization of copper-hydrogen peroxide film growth kinetics". *Thin Solid Films* **2006**, *513*, 311-318.
9. Kunze, J.; Maurice, V.; Klein, L. H.; Strehblow, H. H.; Marcus, P.. "In situ STM study of the duplex passive films formed on Cu (111) and Cu (001) in 0.1 M NaOH". *Corros. Sci.* **2004**, *46*, 245-264.

10. Reed, D. T.; Swayambunathan, V.; Tani, B. S.; Van Konynenburg, R. A.. "Corrosion product identification and relative rates of corrosion of candidate metals in an irradiated air-steam environment". *Proc. Mat. Res. Soc. Symp.* **1989**, 176, 517-524.
11. Reed, D. T.; Van Konynenburg, R. A.. "Corrosion of copper-base materials in irradiated moist air systems". *Proc. Mat. Res. Soc. Symp.* **1991**, 212, 317-325.
12. Glass, R. S.; Konyenburg, R. A. V.; Overturf, G. E.. "Corrosion processes of austenitic stainless steels and copper-based materials in gamma-irradiated aqueous environments", Corrosion, Houston, Texas, 1985.
13. Shreir, L. L.. "Corrosion". Second ed.; Newnes-Butterworths: London, 1976.
14. King, F.; Kolar, M.. "Corrosion of Copper Containers Prior to Saturation of a Nuclear Fuel Waste Disposal Vault"; AECL-11718; Atomic Energy Canada Limited: Pinawa, Manitoba, 1997.
15. Frost, R. L.. "Raman spectroscopy of selected copper minerals of significance in corrosion". *Spectrochim. Acta, Part A* **2003**, 59 (6), 1195-1204.
16. Ropret, P.; Kosec, T.. "Raman investigation of artificial patinas on recent bronze – Part I: climatic chamber exposure". *J. Raman Spectrosc.* **2012**, 43 (11), 1578-1586.
17. Chiavari, C.; Rahmouni, K.; Takenouti, H.; Joiret, S.; Vermaut, P.; Robbiola, L.. "Composition and electrochemical properties of natural patinas of outdoor bronze monuments". *Electrochim. Acta* **2007**, 52 (27), 7760-7769.

Table 1: EDX data recorded on the cross-section of a patch on an irradiated sample after 104 days of exposure. The locations analyzed are numbered in Figure 5.

| | C K (at. %) | O K (at. %) | Cl K (at. %) | Si K (at. %) | Cu L (at. %) |
|--------|-------------|-------------|--------------|--------------|--------------|
| Spot 1 | 5.25 | 36.28 | 1.27 | | 57.20 |
| Spot 2 | 5.98 | 22.81 | 1.38 | 1.55 | 68.37 |

Table 2: EDX data recorded on the cross-section of a patch on a non-irradiated sample after 104 days of exposure. The locations analyzed are numbered in Figure 6.

| | C K (at. %) | O K (at. %) | Cl K (at. %) | Cu L (at. %) |
|--------|-------------|-------------|--------------|--------------|
| Spot 1 | 7.90 | 28.06 | 1.03 | 63.00 |
| Spot 2 | 12.12 | 16.82 | 1.48 | 69.59 |
| Spot 3 | 13.41 | 18.03 | 1.15 | 67.40 |
| Spot 4 | 8.00 | | | 92.00 |

Table 3: Oxidation states of Cu in the corrosion products on a numbered of locations determined by XPS.

| | Cu(0)+Cu(I) | Cu(II) |
|-------------------------------------------|-------------|--------|
| 104 d irradiated – general area | 25 | 75 |
| 104 d irradiated – upper left patch | 27 | 73 |
| 104 d non-irradiated – general area | 24 | 76 |
| 104 d non-irradiated - patch | 23 | 77 |
| Baseline study 90 d sample – general area | 13 | 87 |
| Baseline study 90 d sample – patch | 14 | 86 |

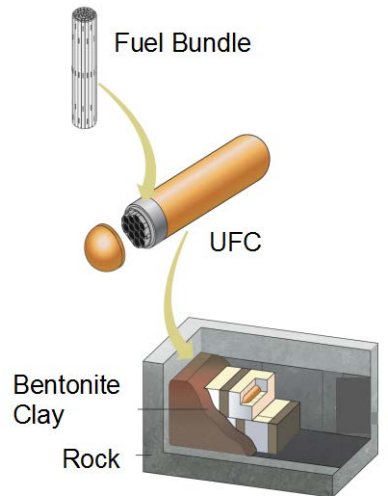


Figure 1: A schematic illustration of the multiple-barrier system proposed for the permanent disposal of spent nuclear fuel in a Deep Geologic Repository.

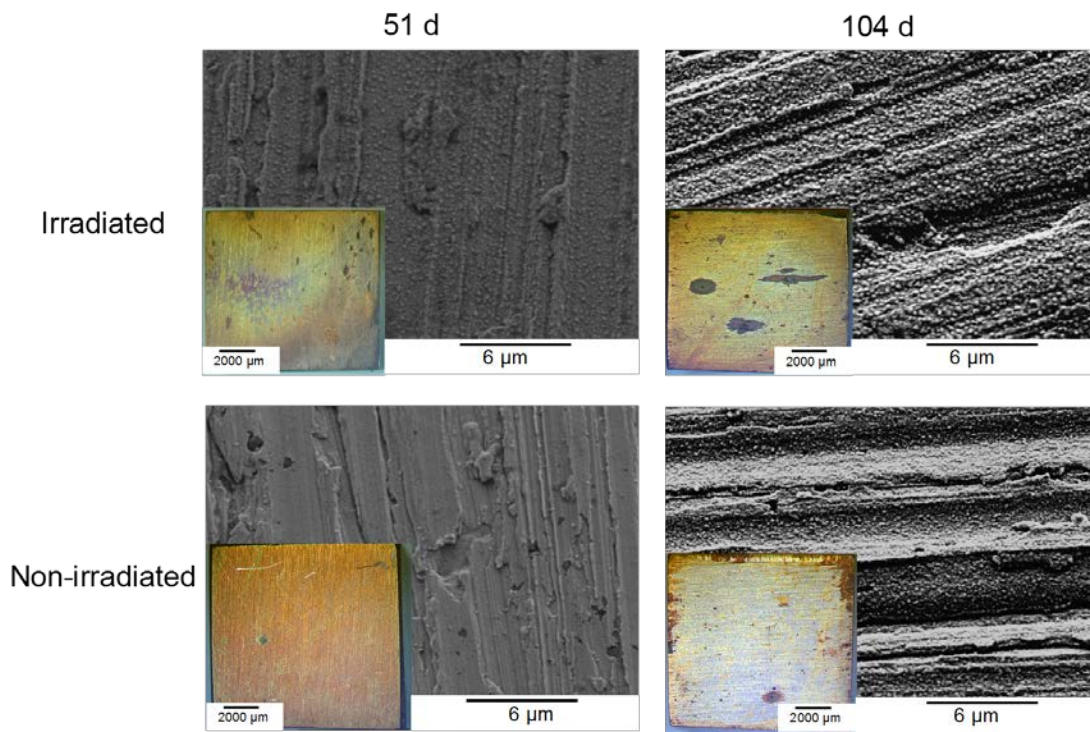


Figure 2: SEM micrographs of the surfaces of coupons exposed in the radiation experiment for different periods showing corrosion of the general areas (copper coloured) in the corresponding optical images.

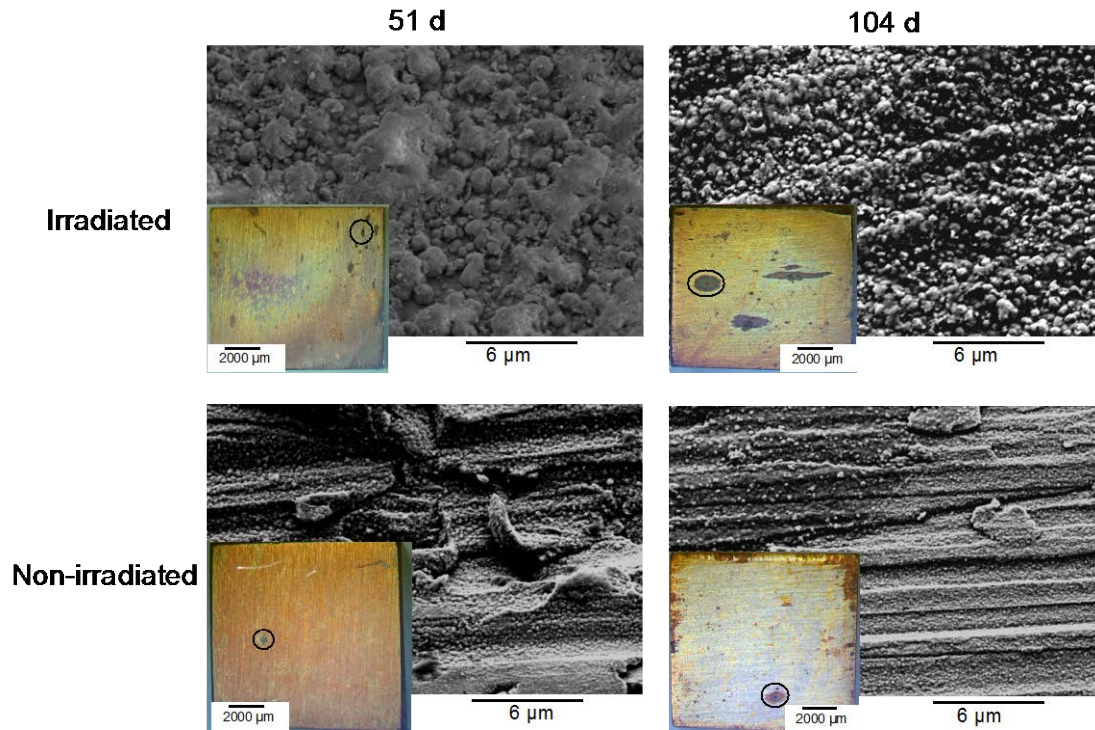


Figure 3: SEM micrographs of the surfaces of samples exposed in the radiation experiment for different periods showing the corrosion within the patches marked with circles in the optical images.

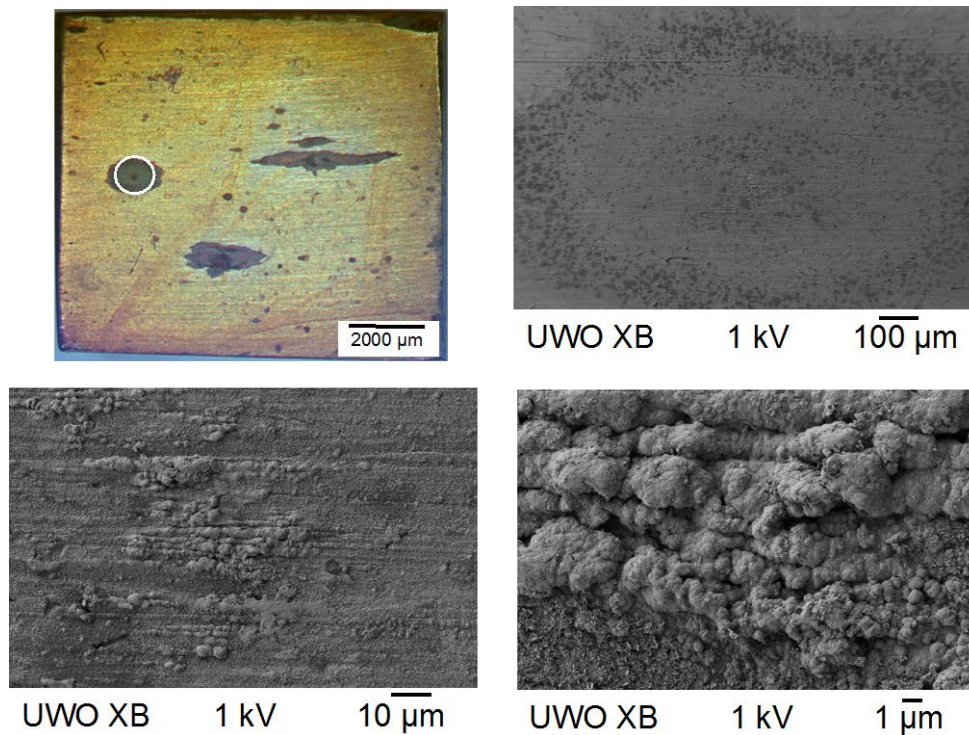


Figure 4: Optical images and SEM micrographs recorded on a sample exposed to irradiated vapour for 104 days. The circled patch shows the locations examined by SEM. The morphology of the corrosion product in the central dark spot can be observed.

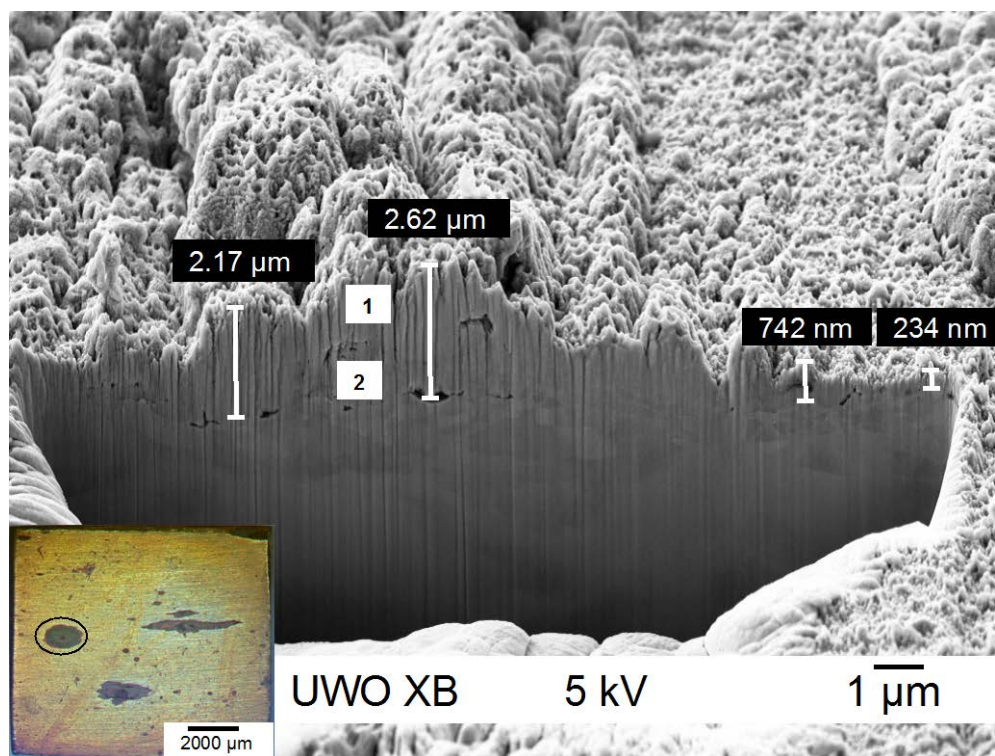


Figure 5: A FIB cut cross section of an irradiated sample exposed for 104 days. The section was cut from within the circled area shown in the optical image. The numbers in the SEM micrograph indicate the locations analyzed by EDX (Table 1).

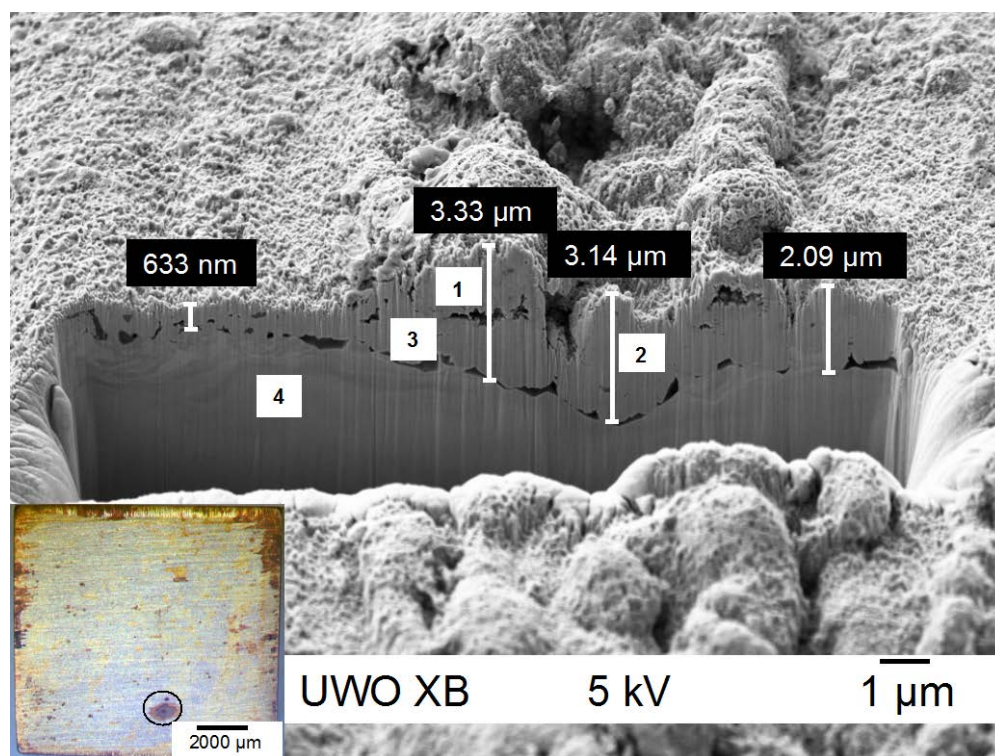


Figure 6: A FIB cut cross section on a non-irradiated sample exposed for 104 days. The section was cut from within the circled area shown in the optical image. The numbers in the SEM micrograph indicate the locations analyzed by EDX (Table 2).

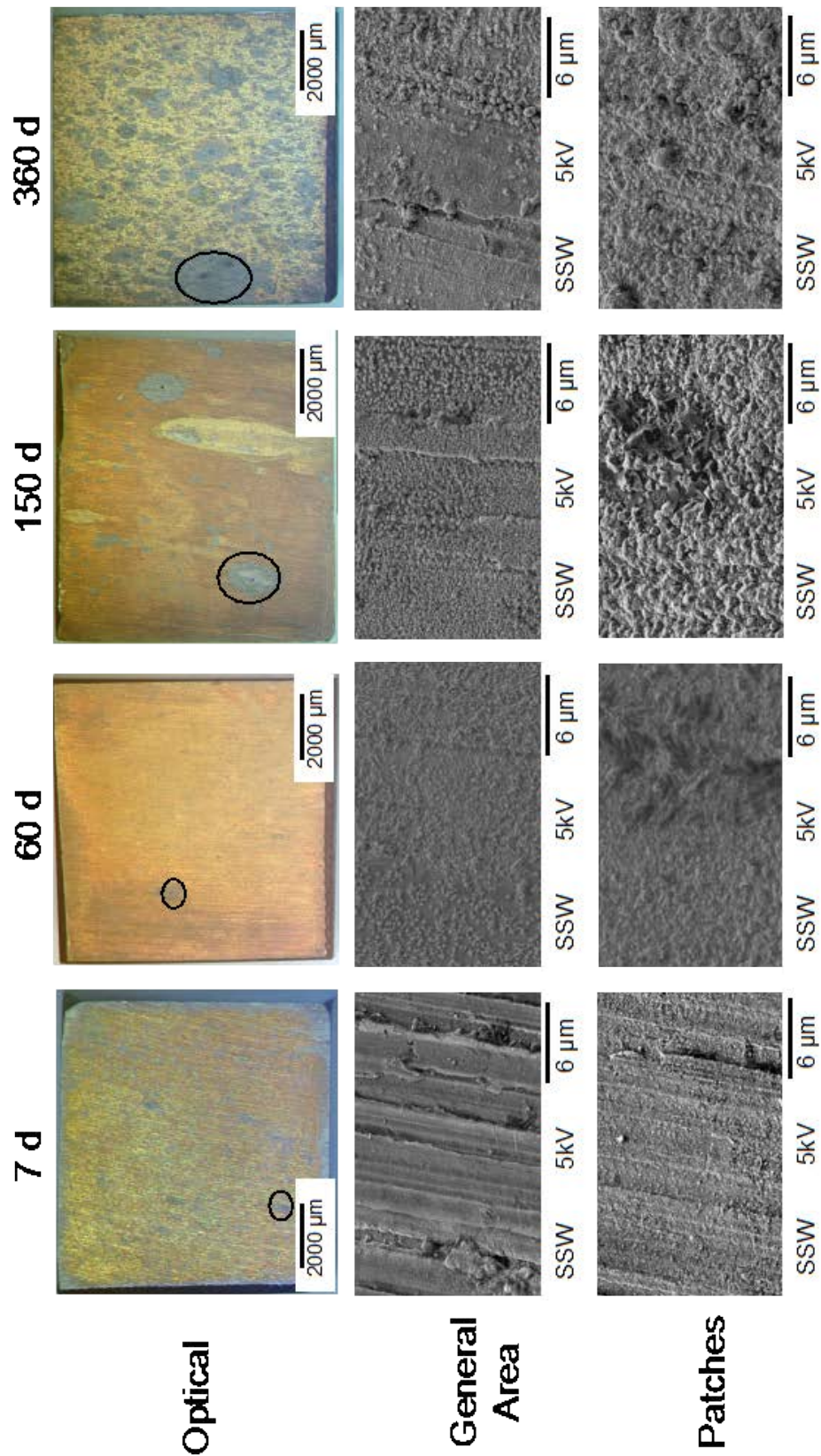


Figure 7: Optical images and SEM micrographs of samples (non-irradiated) removed from the humidity chamber after a number of exposure periods. The circles in the optical images indicate the locations shown in the SEM micrographs.

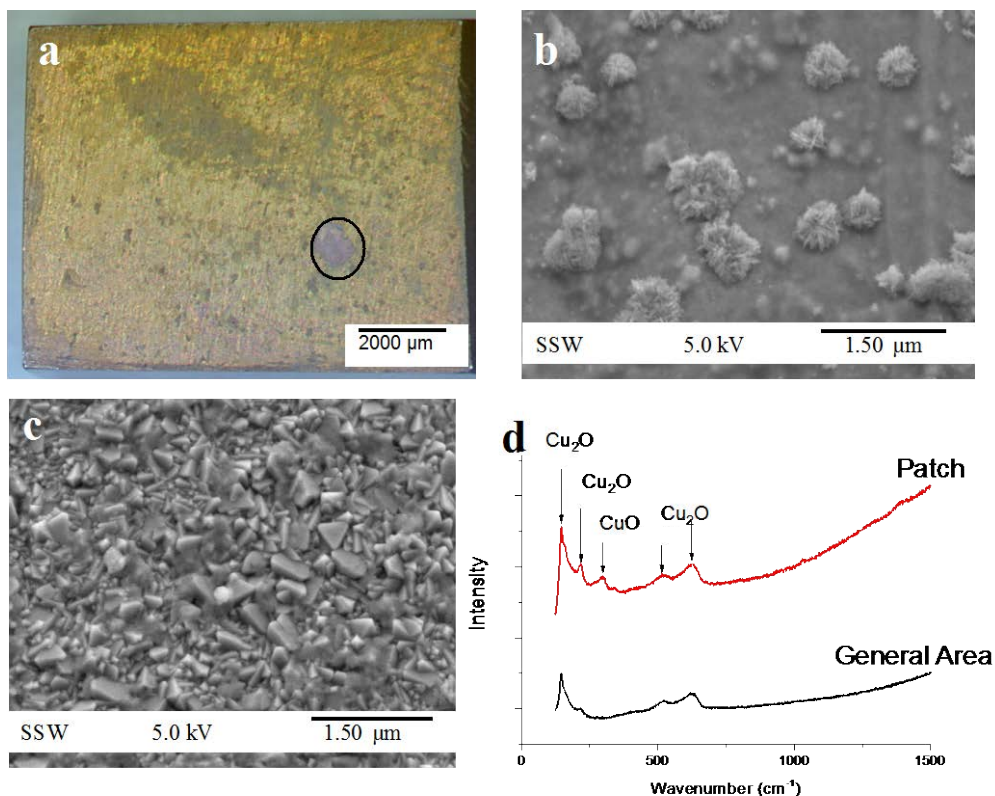


Figure 8: Optical (a), SEM micrographs ((b) and (c)), and Raman spectra (d) recorded on samples (non-irradiated) removed from the humidity chamber after a 30 day exposure. (b) shows the general corroded area: (c) shows the micrograph recorded on the patch marked with a circle in (a). The Raman spectra in (d) are for a general area and a patch.

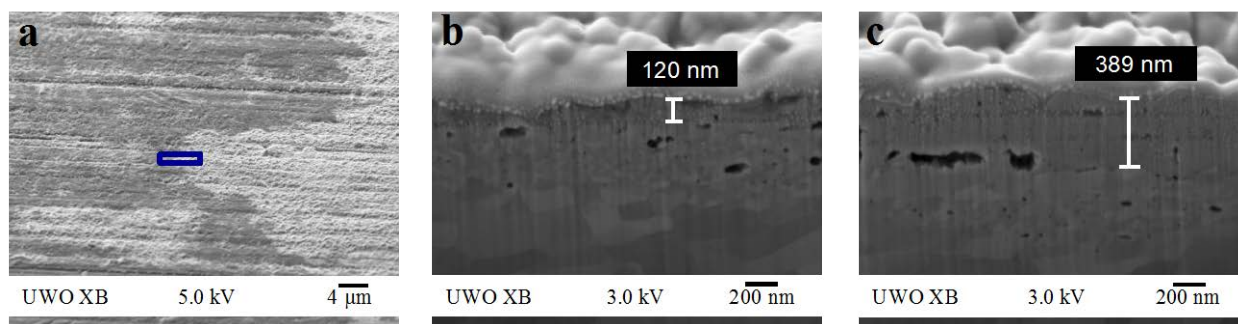


Figure 9: An SEM micrograph (a) recorded on a sample removed from the humidity chamber after a 30 day exposure. (b) and (c) show FIB cut cross sections across a border between a general corrosion area and a patch (the location of the cut is shown in (a): (b) shows the section in a general corroded area; (c) shows the section within the patch.